JACS Au
AN OPEN ACCESS JOURNAL OF THE AMERICAN CHEMICAL SOCIETY

pubs.acs.org/jacsau
Article

Colon-Targeting Supersulfide Donor−Drug Conjugates Align Forces against Inflammation

Yu Zhang,▽ Gao-Yao Cao,▽ Zhihao Zhou, Tian-Yu Hu, Bi-Xin Xu, De-Ao Chen, Jin-Biao Du, Jiankun Wang, Guangji Wang,* and Le Zhen*

Cite This: JACS Au 2025, 5, 642−652
Read Online

ACCESS | Metrics & More | Article Recommendations | Supporting Information

ABSTRACT: Supersulfides are rising stars in regulating redox. Their distinctive redox biological functions are becoming increasingly evident with the advancement of supersulfide donors. However, most existing donors are limited to releasing hydropersulfide (RSSH) only, and in addition, there is still a knowledge gap in translating supersulfides into therapeutic molecules. To this end, in this work, we devised and synthesized a supersulfide donor−drug conjugate, **RSSS−ASA**, containing an azo moiety. This bifunctional prodrug enables the production of hydrotrisulfide (RSSSH) catalyzed by intestinal azoreductase, accompanied by the release of the anti-inflammatory molecule 5-aminosalicylic acid (ASA). Notably, the corelease of the supersulfides with ASA exhibited colonic-targeting attributes, thereby synergistically contributing to the potent anti-inflammatory and antioxidant activities observed in cellular and animal models. This prodrug design is worthy of further development and translation in donor development and disease treatment.

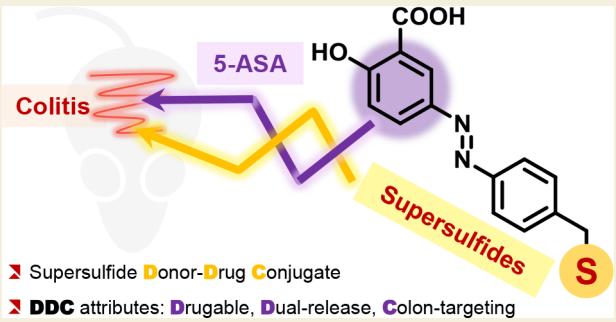

KEYWORDS: *supersulfide, persulfide, colon-targeting, prodrug, colitis, 5-aminosalicylic acid, sulfur metabolome*

INTRODUCTION

The term "supersulfides" has recently been proposed for species containing catenated sulfur atoms (Figure 1b).[1] These

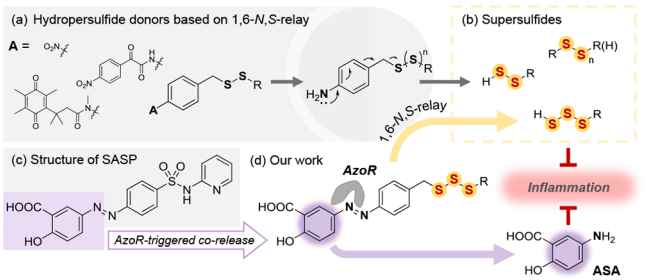

Figure 1. Design of supersulfide donor−drug conjugates based on 1,6-*N*,*S*-relay and AzoR-mediated activation.

sulfur atoms, particularly those with oxidation states of 0 and −1, are highly reactive and labile.[2] They are currently referred to as "sulfane sulfur atoms" embedded in and readily transferred between persulfide and polysulfide species,[3−5] which endows supersulfides with unique structural and functional properties, facilitating the quenching of reactive oxygen species (ROS)/reactive nitrogen species (RNS) and the conversion to hydrogen sulfide (H_2S) for cellular sulfur recycling.[3−8] Their central and versatile role enables supersulfides to construct a buffer system indispensable for maintaining cellular redox homeostasis. Supersulfides have recently been recognized as fascinating molecules that play various regulatory and protective roles in redox-mediated cellular dysfunction and pathological processes relative to oxidative stress.[9−13]

Targeted and controlled delivery of supersulfides into tissues or cells is an emerging topic that warrants further investigation. Hydropersulfide (RSSH) donors have been designed for the direct release of RSSH, the most representative supersulfide, in response to various physiological conditions (pH, esterases, thiols, etc.)[14−24] or biomarkers upregulated in disease (ROS, RNS, NQO1, etc.) (Figure 1a).[25−33] These donors have emerged as potent regulators of supersulfide homeostasis, demonstrating superior antioxidant and cytoprotective effects, particularly distinct biofunctions specific to supersulfides. In certain instances, these donors are more effective than H_2S donors.[34,35] Furthermore, an increasing body of research indicates that supersulfides, rather than H_2S, play a significant role in numerous biological events.[5,9−12,36,37] Consequently, supersulfide donors will be a pivotal tool along with H_2S

Received: September 19, 2024
Revised: January 17, 2025
Accepted: January 20, 2025
Published: January 30, 2025

Scheme 1. Synthesis of Prodrugs RSS−ASA and RSSS−ASA

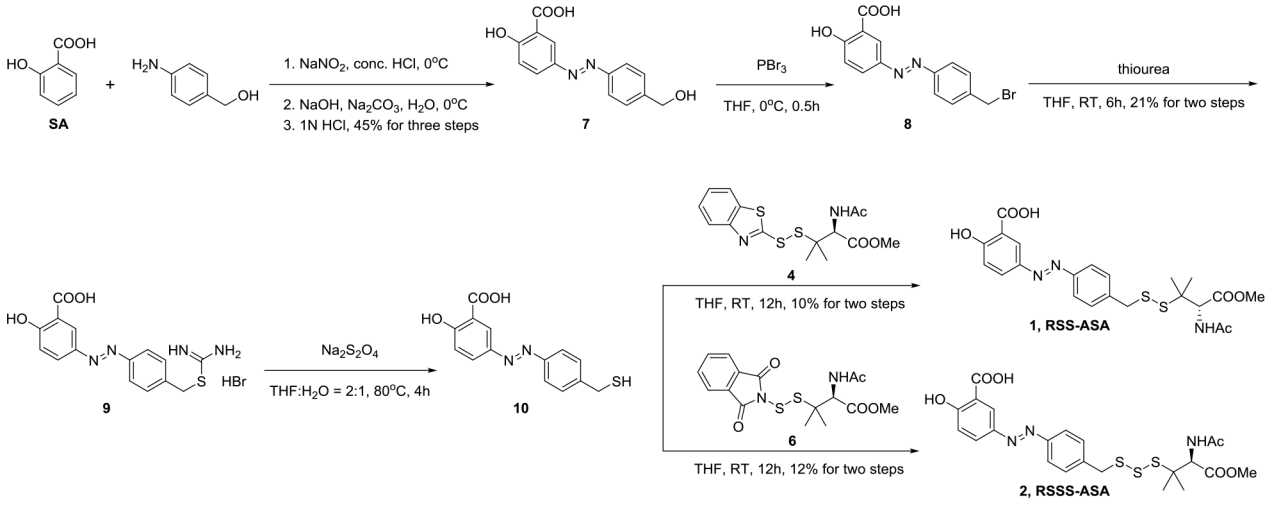

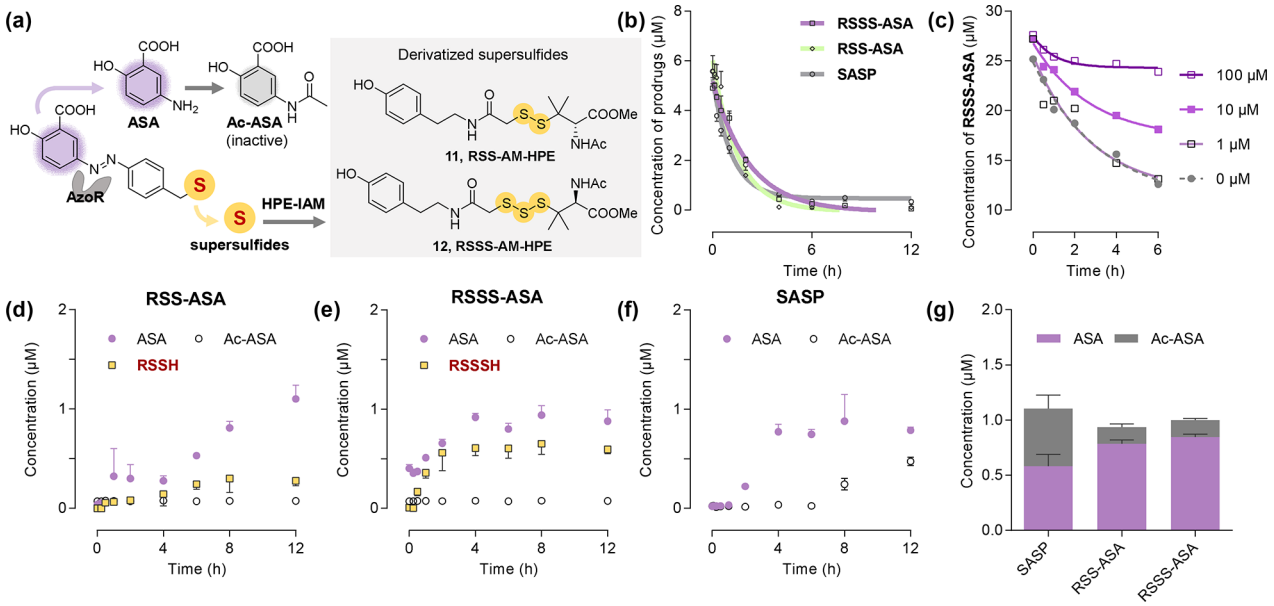

Figure 2. Activation of the prodrugs with the corelease of ASA and supersulfides. (a) AzoR-mediated corelease of ASA and supersulfides. ASA can undergo metabolic conversion to *N*-acetyl-S-ASA (Ac-ASA, an inactive metabolite of ASA), and supersulfides (RSSH and RSSSH) can be converted to **11** and **12**, respectively, in the presence of HPE-IAM. (b) Degradation of prodrugs (5 μM) in a rat colonic content solution (0.1 mg/mL in PBS). (c) Azoreductase (AzoR) inhibitor DPI (0, 1, 10, and 100 μM) blocked the degradation of **RSSS−ASA** (25 μM) in the rat colonic content solution. (d−f) Generation of ASA, Ac-ASA, and supersulfides from 5 μM **RSS−ASA** (d), **RSSS−ASA** (e), or SASP (f) in the rat colonic content solution (0.1 mg/mL in PBS) containing HPE-IAM (50 μM). (g) Supersulfides potentially blocked the metabolic inactivation of ASA. The levels of ASA and Ac-ASA generated from prodrugs (5 μM) was measured following incubation within rat colonic contents (0.1 mg/mL PBS) for 24 h. Data represent the average ± SD (n = 3).

donors in future sulfur biology research, guiding novel therapeutic breakthroughs for preventing and treating diseases with disturbed redox homeostasis.

However, existing supersulfide donors are limited to releasing RSSH. Compared to RSSH, hydrotrisulfide (RSSSH) is a more mysterious molecule that harbors an additional zerovalent sulfur atom, which is an alternative avenue to reprogram the supersulfide pool and potentially more beneficial in combating oxidative stress damage. However, delivering RSSSH more directly remains a challenge. Reported RSSH donors often bear self-immolation linkers undergoing a 1,4- or 1,6-elimination or an intramolecular cyclization. In light of these linkers, we designed RSSSH donors capable of releasing RSSSH through 1,6-elimination[25,28,29,31,33] (Figure 1d).

On the other hand, pursuing more diversified supersulfide donors is ultimately aimed at elucidating their biological activities and applying them in disease treatment. Inspired by the fact that donors of gaseous signaling molecules have demonstrated enhanced clinical therapeutic efficacy when coupled with another drug (e.g., the nitric oxide-donating latanoprostene bunod and the H_2S-donating ATB-429),[38,39] we designed supersulfide donor−drug conjugates (DDCs) (Figure 1d), a novel class of prodrugs capable of coreleasing supersulfides accompanied by a second pharmacologically active molecule. We also validated their pharmacological activity at both the cellular and the animal levels.

https://doi.org/10.1021/jacsau.4c00868
JACS Au 2025, 5, 642−652

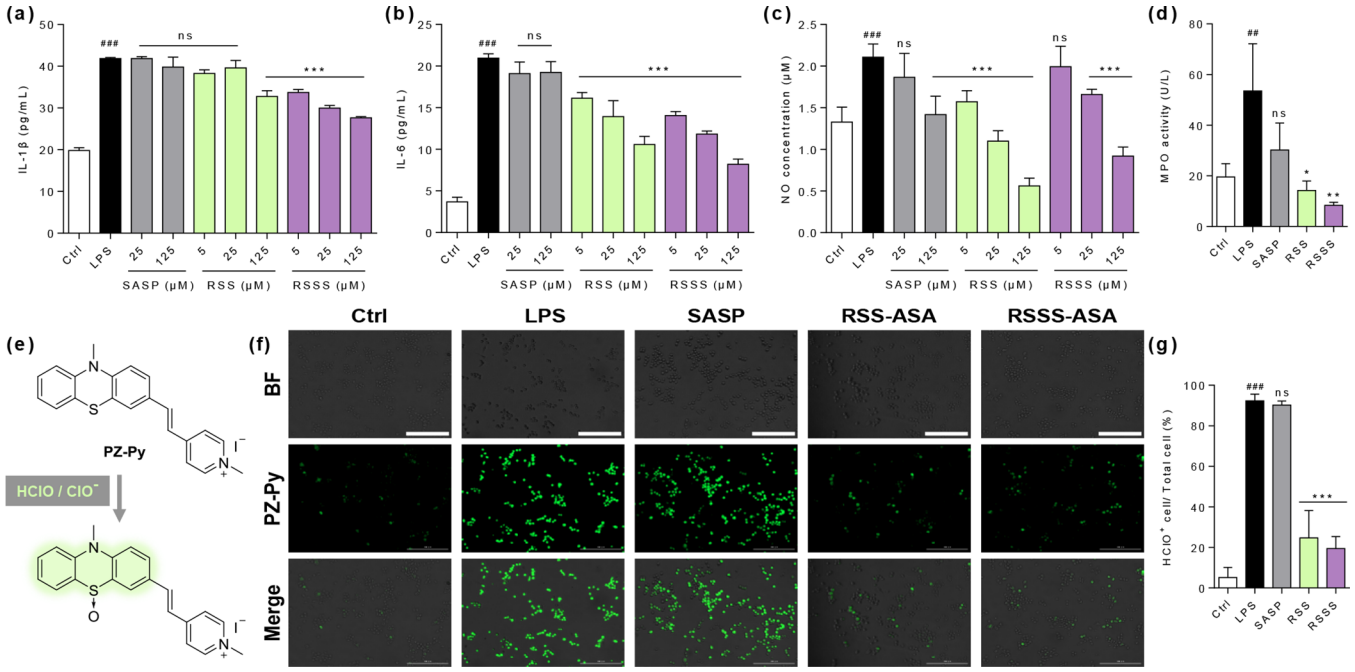

Figure 3. Anti-inflammatory and antioxidant activities of prodrugs on LPS-stimulated RAW 264.7 macrophage cells. (a−d) Effects of SASP, **RSS−ASA** (RSS), and **RSSS−ASA** (RSSS) on the LPS-induced inflammatory response. RAW264.7 cells were pretreated with different concentrations of prodrugs (5, 25, and 125 μM) and LPS (1 μg/mL) for 24 h. IL-1β (a) and IL-6 (b) secretion in the culture supernatant were measured using ELISA. NO production (c) and MPO activity (d) in the culture supernatant were measured. (e) The fluorescent probe Pz−Py was utilized as a sensor of endogenous hypochlorous acid (HClO). (f, g) Representative fluorescent images (f) and quantitative analysis (g) of intracellular HClO. **RSS−ASA** and **RSSS−ASA** attenuated the cellular HClO accumulation induced by LPS. Fluorescence intensity is depicted as a ratio compared to the control group; scale bars = 200 μm. Data represent the mean ± SD of independent experiments (n = 6). ***p < 0.001, **p < 0.01, and *p < 0.05 versus the model group; ###p < 0.001 and ##p < 0.01 versus the control group; ns, not significant.

The azo bond introduced in the prodrugs could be cleaved reductively by azoreductase (AzoR) from colonic bacteria,[40,41] liberating the therapeutic molecule 5-aminosalicylic acid (ASA) and an aniline scaffold. The latter undergoes 1,6-elimination, resulting in the release of supersulfides (RSSH or RSSSH) (Figure 1). Our AzoR-responsive prodrugs were derived from the metabolism of the therapeutic drug sulfasalazine (SASP) (Figure 1c), which releases ASA into the inflamed colon in a spatially selective manner. However, the metabolic byproduct sulfapyridine is responsible for some side effects of SASP.[42,43] In light of these considerations, the newly designed prodrugs, while acquiring colon-targeting properties, also attempt to exert an additive or synergistic effect in inhibiting inflammation through the additional release of supersulfides. Furthermore, this locally acting mode would be more reasonable and practical for exploring the in vivo therapeutic effects of supersulfides, which could circumvent their metabolic stability.

RESULTS AND DISCUSSION

The initial step involved the synthesis of two prodrugs (Scheme 1). Following the diazotization reaction, *p*-aminobenzyl alcohol was coupled to the *para*-position of the phenolic hydroxyl group of salicylic acid to yield benzyl alcohol **7**, which contains an azo structure. Subsequently, after bromination, thiourea substitution, and hydrolysis, thiol **10** was synthesized. The reaction of compound **10** with different active forms of thiols produced prodrugs with varying structures. The reaction with compound **4** yielded the disulfide compound **RSS−ASA** (**1**), whereas the reaction with compound **6** gave rise to the trisulfide compound **RSSS−ASA** (**2**).

After obtaining the prodrugs, the feasibility of the corelease of supersulfide and ASA was verified. The prodrugs (5 μM) were incubated with rat colonic contents (0.1 mg/mL) for 12 h, during which the azo bond was cleaved by bacterial AzoR, producing ASA and triggering supersulfide release (hydropersulfide in the case of **RSS−ASA**; hydrotrisulfide in the case of **RSSS−ASA**). In addition, acetylated ASA (Ac-ASA), a compound considered an inactivated metabolite detrimental to potency, was also examined (Figure 2a).[44] To detect reactive RSSH and RSSSH, the thiol-trapping reagent β-(4-hydroxyphenyl)ethyl iodoacetamide (HPE-IAM) was added to generate derivatives **11** and **12** (Figure 2a), facilitating the stabilization and quantification of the supersulfides (Scheme S5). The release process was quantitatively outlined by liquid chromatography-tandem mass spectrometry (LC-MS/MS) for each of the aforementioned product. Prodrugs **RSS−ASA** and **RSSS−ASA** degraded at rates comparable to that of the control drug SASP (Figures 2b and S1, S2), which was blocked by the AzoR inhibitor diphenyleneiodonium chloride (DPI) (Figure 2c), indicating that AzoR is essential for the prodrug activation in a reaction system containing colonic contents. Along with prodrug decomposition, the accumulation of both supersulfide species and ASA was observed (Figure 2d−f). All three prodrugs exhibited comparable yields of ASA over time. Notably, after 12 h of coincubation, RSSS−ASA released RSSSH in 13% yield, which was 0.7 times that of ASA (19% yield), and this release efficiency was superior to that of RSS−ASA for RSSH (6% yield, which was only 0.27 times that of ASA release). The lower release efficiency of RSSH/RSSSH than that of ASA is partly due to the immediate formation of ASA after azo bond cleavage, whereas supersulfide release

https://doi.org/10.1021/jacsau.4c00868
JACS Au 2025, 5, 642−652

requires a 1,6-elimination process, which is the rate-limiting step from the experimental results and available reports.[25,28] In the case of similar ASA yields, the higher yield of RSSSH reflected that the trisulfide may be more susceptible to 1,6-elimination than the disulfide, but this intriguing result needs to be further investigated in subsequent experiments. Overall, the low yields of both ASA and RSSSH may be due to the complexity of the colonic contents, which contain metabolic enzymes and thiols that may affect the stability of the prodrugs and their metabolites.

The conversion of ASA to Ac-ASA is mediated by *N*-acetyltransferases (NATs) in bacterial or intestinal tissues and is closely linked to the efficacy of ASA.[45] All three prodrugs yielded the inactive metabolite Ac-ASA over the course of the 12 h reaction, with the SASP group producing the highest amount. Upon extending the coincubation period to 24 h, the ratio of ASA to Ac-ASA generated by SASP was close to 1:1. In stark contrast, prodrugs **RSS−ASA** and **RSSS−ASA** yielded markedly higher proportions of ASA (Figure 2g), indicating that the supersulfides may be responsible for the observed reduction in metabolic inactivation. The NAT-mediated acetyltransfer depends on a crucial cysteine residue in the catalytic center of acetyltransferase.[46] As supersulfides may covalently modify sulfhydryl groups in proteins,[47] we postulated that the RSSH or RSSSH released from the prodrug might covalently inhibit the NAT enzyme activity, thereby blocking ASA acetylation.

The in vitro anti-inflammatory and antioxidant activities of the prodrugs were evaluated after confirming the corelease of two bioactive molecules. LPS-stimulated macrophage RAW264.7 cells were used as a cellular model of inflammation, wherein the levels of the inflammatory factors IL-1β, IL-6, and NO were elevated in the cell supernatants (Figure 3a−c). The secretion of these factors was minimally inhibited by SASP. In contrast, prodrugs **RSS−ASA** and **RSSS−ASA** provided substantial relief from the LPS-induced overproduction of inflammatory factors without cytotoxicity (Figure S4). Myeloperoxidase (MPO) is a critical enzyme found in neutrophils and macrophages, responsible for hypochlorous acid (HClO) production from hydrogen peroxide and chloride ions.[48] Excessive HClO, as a powerful ROS, often results in uncontrolled inflammation.[49] Our findings demonstrate that the two supersulfide donors effectively suppressed MPO activity within cellular supernatants, while SASP exhibited no inhibitory effect (Figure 3d). Subsequently, the fluorescent probe **PZ−Py** was employed as an indicator of intracellular HClO (Figure 3e).[50] Consistent with the observed reduction in the extracellular MPO activity, intracellular HClO was also significantly scavenged following the administration of the supersulfide donors (Figure 3f,g). The cellular anti-inflammatory and antioxidant activities of the two prodrugs are significantly superior to those of SASP. The prodrugs can be activated by the mammalian AzoR contained in RAW264.7 cells.[40] However, the azo structure alone is insufficient to produce an adequate anti-inflammatory effect. The disulfide or trisulfide structures of the prodrugs contribute significantly to the observed activity.

The intracellular generation of supersulfides was characterized (Figure 4). Following a 2 h prodrug treatment with RAW264.7 cells, methanol containing HPE-IAM was used to extract and simultaneously stabilize intracellular supersulfides. The results showed the absence of supersulfide derivatives (**11** or **12**) in the untreated and SASP groups. **RSS−ASA** exhibited

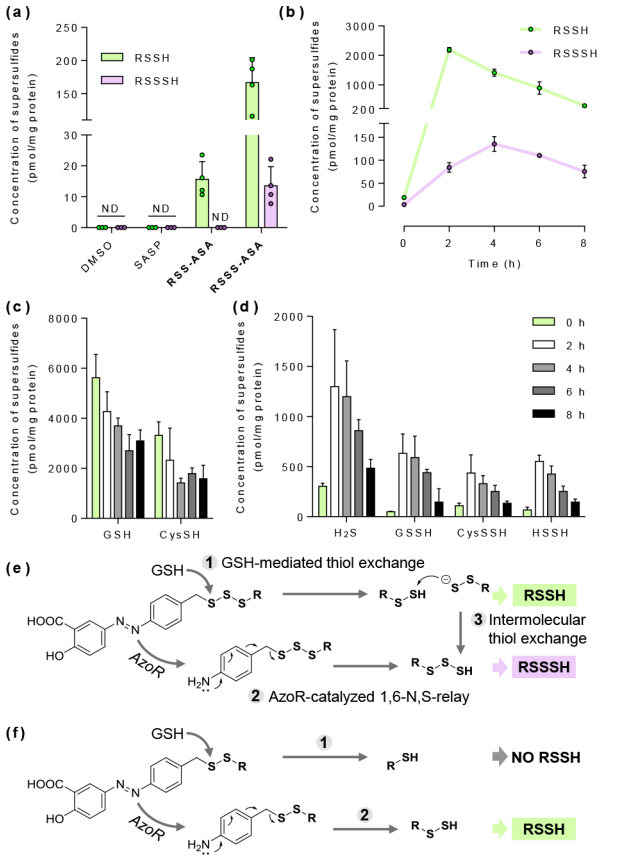

Figure 4. (a, b) Intracellular supersulfide release. RAW 264.7 cells were pretreated with (a) prodrugs (150 μM for 2 h) or (b) **RSSS−ASA** (150 μM for 0, 2, 4, 6, and 8 h). (c, d) Changes in the endogenous thiol (GSH, CysSH, and H_2S) and supersulfide (GSSH, CysSSH, and HSSH) contents triggered by the exogenous supersulfides supplied in (b). The supersulfides were analyzed by LC-MS/MS followed by extraction with methanol containing HPE-IAM. Data represent the average ± SD (n = 4). (e, f) Brief mechanism of generation of supersulfides by **RSSS−ASA** (e) and **RSS−ASA** (f).

a limited capacity to release sufficient RSSH in cells. Interestingly, **RSSS−ASA** generated both RSSH and RSSSH intracellularly, with the concentration of the former approaching 10-fold that of the latter (Figure 4a). Subsequently, following the optimization of the sample collection and extraction methods to address the suspension tendency of RAW264.7 cells, an investigation was conducted into the content of the two supersulfides produced intracellularly by **RSSS−ASA** over time (Figure 4b). The intracellular concentrations of RSSH and RSSSH demonstrated an initial increase, followed by a subsequent decline. The highest concentration of RSSH was observed at 2 h, while RSSSH reached its maximum at 4 h. The maximum concentrations of RSSH and RSSSH were approximately 2000 and 130 pmol/mg of protein, respectively. Notably, the substantial introduction of exogenous supersulfides into the cell altered the composition of representative endogenous thiols and supersulfides (Figure 4c,d). The levels of glutathione (GSH) and cysteine (Cys) exhibited a declining trend, which may be attributed to the fact that the prodrugs or their metabolites readily react with these two thiols intracellularly, resulting in a depletion of thiols. Conversely, for H_2S and supersulfides such as glutathione persulfide (GSSH), cysteine persulfide (CysSSH), and hydrogen persulfide (HSSH), the content of

https://doi.org/10.1021/jacsau.4c00868
JACS Au 2025, 5, 642−652

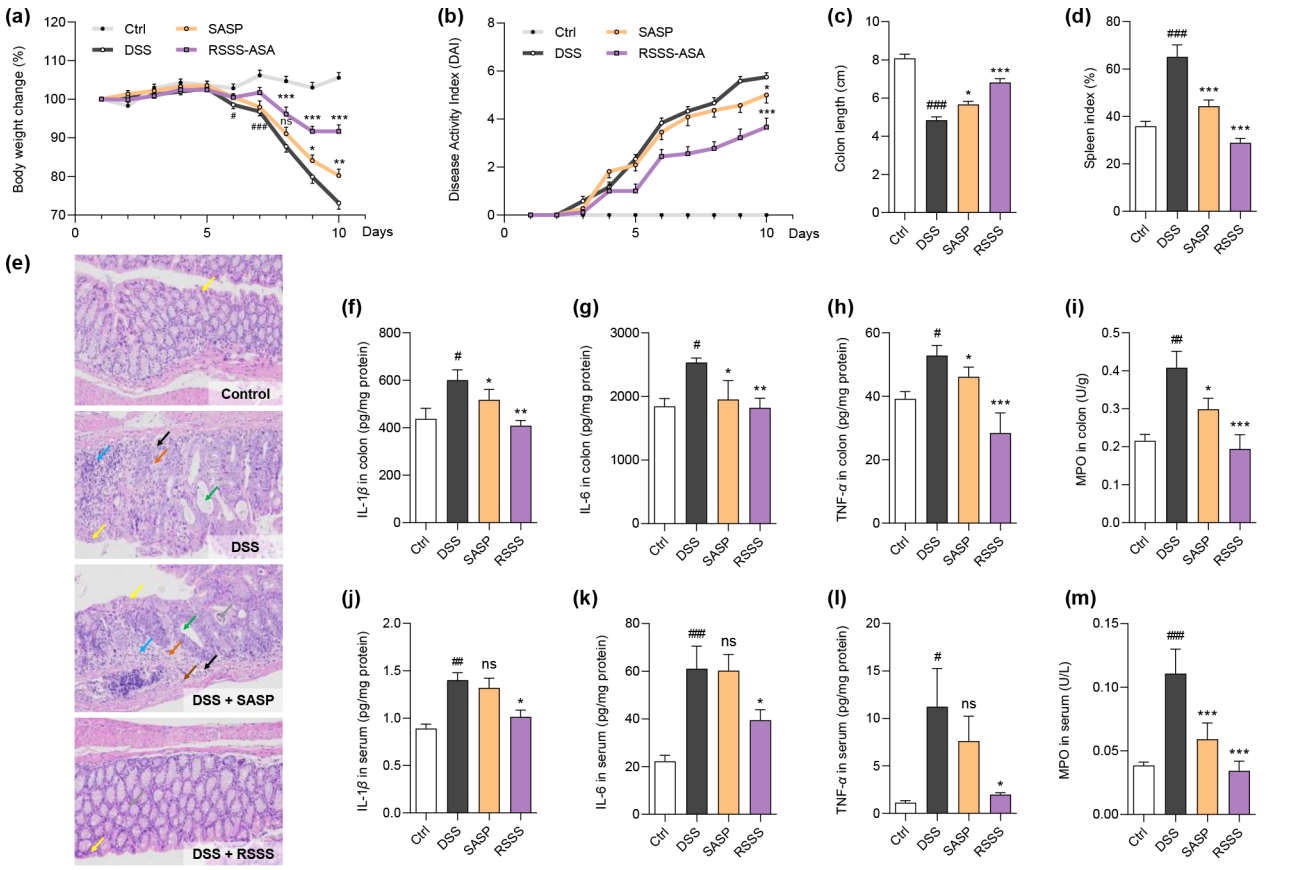

Figure 5. RSSS−ASA attenuated dextran sulfate sodium (DSS)-induced colitis in mice. (a−d) Changes in body weight (a), disease activity index (DAI) (b), colon length (c), and spleen wet weight index (d) of C57BL/6 mice challenged with DSS (2.5%) during 10 days. (e) Histological changes following oral administration of **RSSS−ASA** or SASP in the DSS-induced colitis mouse model. Colon tissue was paraffin-embedded and analyzed by H&E staining. (f−m) Detection of inflammatory cytokines and MPO activity. The levels of IL-1β (f), IL-6 (g), TNF-α (h), and MPO activity (i) in the colon tissue. The levels of IL-1β (j), IL-6 (k), TNF-α (l), and MPO activity (m) in the serum. The mice were treated with DSS at a concentration of 2.5% in drinking water for 8 days followed by 2 days of recovery with DSS-free water. **RSSS−ASA** (0.2 mmol/kg) or SASP (0.2 mmol/kg) was orally administered once a day for 10 days. Data represent mean ± SD of independent experiments ($n = 6$). ***$p < 0.001$, **$p < 0.01$, and *$p < 0.05$ versus the DSS group; $^{###}p < 0.001$ and $^{#}p < 0.05$ versus the control group; ns, not significant.

prodrugs was significantly elevated to 4 to 10 times their original content in the cell. The production of supersulfides from **RSSS−ASA** can be divided into three main pathways (Figure 4e). (1) GSH-mediated thiol-exchange reactions result in the direct production of RSSH. (2) The prodrug undergoes AzoR-catalyzed azo bond cleavage, which drives the direct RSSSH release triggered by 1,6-*N*,*S*-relay. (3) The thiol-exchange reactions between RSSH molecules result in the indirect formation of RSSSH. In contrast, the classical **RSS−ASA** scaffold is only present in pathway (2) (Figure 4f), and the results suggest that this pathway does not contribute significantly to the prodrug activation. This finding may be attributed to the fact that the thiol-exchange reaction between trisulfides and endogenous thiols occurred more readily, whereas the intracellular AzoR activation was not dominant due to enzyme abundance and reactivity. **RSSS−ASA** demonstrated the capacity to directly deliver at least two highly reactive sulfur species, representing the first instance of intracellular RSSSH delivered at such a high concentration by artificial donors.

To further investigate the therapeutic advantages of the novel prodrugs, **RSSS−ASA** was evaluated in the DSS-induced mouse colitis model with SASP serving as a control compound. Mice were gavaged with equimolar doses of **RSSS−ASA** and SASP (0.2 mmol/kg) for 10 consecutive days. DSS (2.5%) was added to drinking water, except for the control group. As illustrated in Figure 5a, mice in the DSS group exhibited a notable reduction in body weight from the sixth day of DSS treatment in comparison to the control group. Conversely, both **RSSS−ASA** and SASP demonstrated the capacity to mitigate weight loss in mice, with **RSSS−ASA** exhibiting a more pronounced effect on weight maintenance. The DSS-induced colitis in mice was accompanied by diarrhea and rectal bleeding, which were assessed using the disease activity index (DAI). The DAI scores presented a gradual elevation as the colitis modeling progressed in the DSS group. However, mice that received the prodrugs exhibited milder symptoms and lower DAI scores, particularly in the **RSSS−ASA** group (Figure 5b). Compared to the control group, DSS-induced colitis in mice is characterized by a shortened colon and splenic enlargement. **RSSS−ASA** demonstrated superior efficacy in mitigating pathologic alterations and promoting disease recovery compared to SASP (Figure 5c,d).

Subsequent pathological examination of the colon tissue was performed by H&E staining (Figure 5e). Colon sections from control mice showed intact intestinal structures, and sections from DSS-induced colitis mice showed severe mucosal damage and inflammatory cell infiltration. Compared with the model

https://doi.org/10.1021/jacsau.4c00868
JACS Au 2025, 5, 642−652

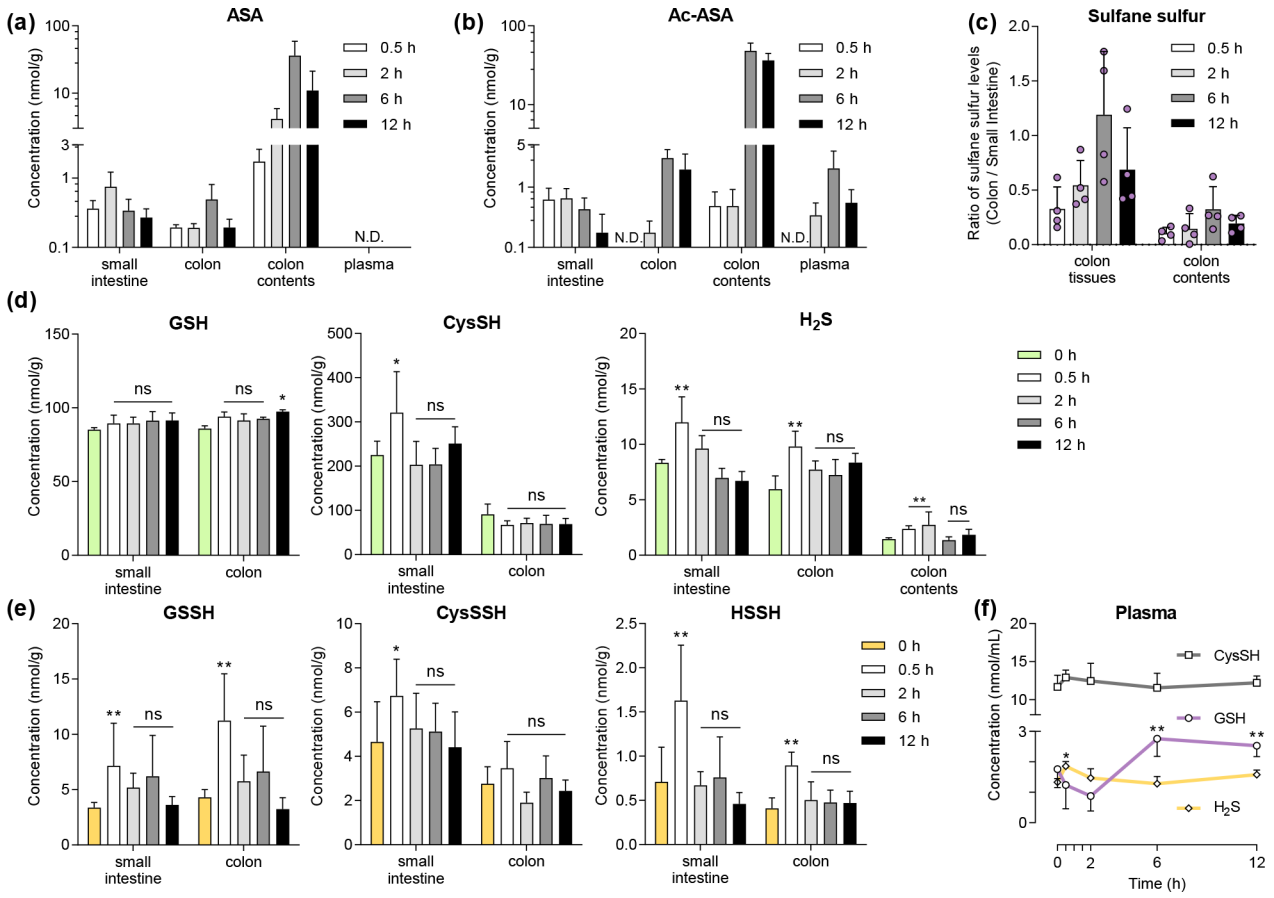

Figure 6. RSSS−ASA (0.1 mmol/kg) enables the corelease of ASA with supersulfides in the mouse colon. (a, b) Intestinal distribution of ASA (a) and the inactivated metabolite Ac-ASA (b) in the small intestine, colon, and colonic contents, as well as their exposure in plasma at different time points (0.5, 2, 6, and 12 h). Tissue concentration is given in nmol/g; plasma concentration is given in nmol/mL. (c) Ratio of colonic sulfane sulfur relative to small intestinal sulfane sulfur. N.D., not detected. Data represent the mean ± SD of independent experiments (n = 4). (d−f) Time-dependent changes in the intestinal (d, e) and plasma (f) levels of endogenous thiols (GSH, CysSH, and H_2S) and supersulfides (GSSH, CysSSH, and HSSH) after the administration of **RSSS−ASA**. The supersulfides were analyzed by LC-MS/MS followed by extraction with methanol containing HPE-IAM. Data represent the average ± SD (n = 4). **p < 0.01 and *p < 0.05 versus the 0 h group; ns, not significant.

mice, mice in the **RSSS−ASA** group showed only mild mucosal damage and pathological changes, and mice in the SASP group still showed some degree of tissue structure damage and inflammatory cell infiltration. The production of inflammatory factors in the colon was quantified by an enzyme-linked immunosorbent assay (ELISA). DSS induction significantly increased the secretion of inflammatory cytokines IL-1β, IL-6, and TNF-α in the mouse colon compared to the control group. **RSSS−ASA** intervention significantly inhibited the production of these three inflammatory factors, whereas the inhibitory effect of SASP was less pronounced (Figure 5f−h).

In the serum, **RSSS−ASA** significantly inhibited the secretion of inflammatory factors, while SASP was less effective (Figure 5j−l). MPO is a newly identified biomarker of colitis, and MPO-mediated oxidative damage exacerbates disease progression.[48,49] DSS induction exacerbated MPO activity in both the colon and serum, and the administration of both SASP and **RSSS−ASA** effectively reduced the MPO activity, with **RSSS−ASA** being more potent (Figure 5i,m).

The remarkable protection of the prodrug **RSSS−ASA** against colitis may originate from the synergistic effect of supersulfides and ASA. Accordingly, further investigation was warranted to elucidate the in vivo prodrug activation in spatial and temporal dimensions. The degradation of **RSSS−ASA** was not observed at different pH levels, indicating its chemical stability in simulated gastrointestinal media (Figure S3). **RSSS−ASA** was undetectable in both the intestine and plasma following a single oral administration (0.1 mmol/kg), suggesting that the prodrug was rapidly biotransformed in the gut. The generation of ASA was detected in the small intestine, colon, and colonic contents (Figure 6a). The time to maximum concentration of ASA in the small intestine was 2 h, while in the colonic site (both tissues and contents), the concentration peaked at 6 h and then decreased. The absence of ASA in plasma resulted in a specific tissue distribution with an optimal intestinal/blood ratio. With regard to Ac-ASA, the inactive metabolite, the trend in tissue distribution was comparable to that observed for ASA, except that its exposure was detectable in plasma (Figure 6b). Regrettably, RSS-AM-HPE (**11**) and RSSS-AM-HPE (**12**) were not identified in intestinal tissues, which was attributed to the rapid exchange of the trisulfide structure with abundant endogenous thiols and the generation of multiple sulfur-containing compounds, which prevented the use of RSSH and RSSSH derivatives as references for LC-MS/MS quantification. Furthermore, we discovered that RSSS-AM-HPE (**12**) was unstable in each test matrix, presenting a significant challenge in its detection.

https://doi.org/10.1021/jacsau.4c00868
JACS Au 2025, 5, 642−652

Consequently, indirect determination of changes in sulfane sulfur and endogenous sulfur metabolomics triggered by the prodrug is now required.

To examine the supersulfide production, the ratio of sulfane sulfur levels in the colon and colonic contents relative to those in the small intestine was respectively determined using the sulfane sulfur probe SSP4 (Figure 6c).[51,52] This ratio, indicative of the colon-targeting levels of supersulfides, increased over time, reaching its peak at the sixth hour. The ratios in colonic contents followed a similar trend but at lower levels. Targeted metabolomics reveals more precise changes in specific representative thiols as well as supersulfides than fluorescence methods for imaging the entire sulfur sulfane pool. After a single dose of **RSSS−ASA**, GSH and CysSH concentrations basically stabilized, with the colonic site showing a slight increase in GSH at 12 h postdosing, and CysSH in the small intestine showed an increase at 0.5 h postdosing. Notably, the administration significantly increased the H_2S levels in the small intestine, colon, and colon contents, and this increase was observed only 0.5 h after administration (Figure 6d). Similarly, the intestinal and colonic levels of supersulfides (GSSH, CysSSH, and HSSH) demonstrated a notable increase at 0.5 h, followed by a return to baseline levels (Figure 6e). Plasma CysSH exhibited minimal fluctuations throughout the administration period. Plasma GSH levels were elevated after 6 and 12 h of administration, while H_2S in plasma mildly increased in the first 0.5 h (Figure 6f). The detection of supersulfides in plasma proved particularly challenging due to the instability of the reference compounds in the matrix. Developing reliable methods would be beneficial to revisiting the levels of these reactive sulfur species. The results indicated that **RSSS−ASA** has the potential to deliver the anti-inflammatory molecule ASA to the colon, while also increasing thiol, H_2S, and supersulfide levels throughout the intestinal tract at a relatively rapid rate. This "two-pronged" mode of action provides a more potent intervention in intestinal inflammation.

CONCLUSIONS

In conclusion, this work developed a novel class of supersulfide DDCs characterized by the colon-targeted corelease of supersulfide with the anti-inflammatory molecule ASA. This corelease was demonstrated to contribute to anti-inflammatory and antioxidant activities in cells and animals, thereby conferring highly promising therapeutic advantages to the prodrug molecules. The present work provides novel insights into donor design from tissue targeting and drug codelivery. The novel DDC pattern will drive a new phase of donor development, evoking the delivery of more diverse supersulfide members and advancing the translation of supersulfides into therapeutic molecules.

METHODS

General Chemistry

Full descriptions of experimental materials and reagents, chemical syntheses (Schemes S1−S4), and analytical methods are provided in the Supporting Information.

Synthesis of 7

To a solution of $NaNO_2$ (1.4 g, 20 mmol) and concentrated HCl (5.5 mL, 150 mmol) was added dropwise a solution of (4-aminophenyl) methanol (2.46 g, 20 mmol) in water (25 mL) at 0 °C for 30 min. Then, the resulting diazonium salt solution was added dropwise into a solution of sodium hydroxide (400 mg, 10 mmol), sodium carbonate (4.18 g, 30 mmol), and salicylic acid (2.76 g, 20 mmol) in water (50 mL). The resulting slurry was stirred at 0 °C for 3 h, which was further quenched with 1 M HCl (20 mL) to adjust the pH to 3−4 and extracted with ethyl acetate (3 × 30 mL). The organic layers were combined, dried over Na_2SO_4, and concentrated. The residue was purified by trituration with dichloromethane to afford the title compound **7** as an orange solid (2.43 g, 45%). ^{1}H NMR (500 MHz, DMSO) δ 8.33 (d, J = 2.6 Hz, 1H), 7.86 (dd, J = 8.8, 2.6 Hz, 1H), 7.80 (d, J = 8.2 Hz, 2H), 7.50 (d, J = 8.1 Hz, 2H), 6.86 (d, J = 8.8 Hz, 1H), 4.60 (s, 2H).

Synthesis of 8

A 50 mL flask was charged with alcohol **7** (272 mg, 1 mmol) in THF (20 mL). To the flask was added dropwise phosphorus tribromide (76 μL, 0.8 mmol), and the resulting solution was stirred for 30 min, which was further quenched with $NaHCO_3$ solution (20 mL). Following the addition of $NaHCO_3$ solution, the reaction was extracted by ethyl acetate (5 × 20 mL). The organic layers were combined, washed with $NaHCO_3$ solution (10 mL) and brine (10 mL), dried over Na_2SO_4, and concentrated in a rotary evaporator. The residue was purified by trituration with dichloromethane to afford the crude product **8** as an orange solid (110 mg), which was used for the next reaction without further purification.

Synthesis of 9

A 20 mL flask was charged with bromine substitute **8** (330 mg, 1 mmol) and THF (5 mL). To the flask was added thiourea (79 mg, 0.8 mmol), and the resulting mixture was stirred for 6 h at room temperature. The solvent was evaporated, and the residue was purified by trituration with dichloromethane to afford the title compound **9** as a yellow solid (254 mg, 21% for two steps). ^{1}H NMR (300 MHz, DMSO) δ 9.17 (d, J = 40.0 Hz, 4H), 8.35 (s, 1H), 8.14−7.97 (m, 1H), 7.88 (s, 2H), 7.63 (s, 2H), 7.13 (d, J = 10.0 Hz, 1H), 4.62 (s, 2H). ^{13}C NMR (126 MHz, DMSO) δ: 171.4, 169.5, 169.1, 152.3, 142.9, 137.4, 130.4, 127.2, 126.5, 122.7, 119.8, 118.2, 34.4. HRMS (ESI) for $C_{15}H_{15}N_4O_3S$ $[M - Br]^+$ calcd 331.0859, found 331.0848.

Synthesis of 10

Thiourea salt **9** (413 mg, 1 mmol) was first suspended in degassed THF (4 mL), to which a solution of $Na_2S_2O_5$ (776 mg, 4 mmol) in H_2O (2 mL) was added in one portion. The reaction was vigorously stirred at 80 °C for 4 h in a sealed tube. The aqueous layer was extracted with EA (3 × 5 mL). The organic layers were combined, washed with brine (10 mL), dried over Na_2SO_4, and concentrated. The crude product was purified by silica gel chromatography (dichloromethane/methanol = 30/1−10/1), affording the orange solid **10**. ^{1}H NMR (500 MHz, DMSO) δ 8.30 (s, 1H), 7.85−7.80 (m, 1H), 7.77 (d, J = 8.3 Hz, 2H), 7.52 (d, J = 8.4 Hz, 2H), 6.81 (d, J = 8.7 Hz, 1H), 3.83 (d, J = 7.8 Hz, 2H), 2.96 (t, J = 7.8 Hz, 1H). The crude product **10** was used directly in the next step as soon as possible to avoid decomposition during purification.

Synthesis of 1 (RSS−ASA)

A two-necked bottom flask was charged with crude thiol **10** (290 mg, 1 mmol) and anhydrous THF (5 mL). Under a nitrogen atmosphere, **4** (370 mg, 1 mmol) in THF (5 mL) was added dropwise. The mixture was stirred at room temperature for 24 h and then concentrated under vacuum. The residue was purified by column chromatography (dichloromethane/methanol = 50/1−10/1) to afford an orange solid (82 mg, 10% for two steps from 1.7 mmol of **9**). ^{1}H NMR (500 MHz, DMSO) δ 8.32 (d, J = 8.7 Hz, 1H), 8.26 (d, J = 2.7 Hz, 1H), 7.80 (d, J = 2.7 Hz, 1H), 7.77 (d, J = 8.3 Hz, 2H), 7.47 (d, J = 8.3 Hz, 2H), 6.75 (d, J = 8.8 Hz, 1H), 4.64 (d, J = 8.7 Hz, 1H), 4.09−3.98 (m, 2H), 3.67 (s, 3H), 1.94 (s, 3H), 1.36 (d, J = 8.9 Hz, 6H). ^{13}C NMR (126 MHz, DMSO) δ: 171.1, 170.9, 170.1, 169.8, 152.0, 142.7, 139.6, 130.6, 127.0, 126.4, 122.5, 118.2, 70.3, 58.6, 52.3, 52.2, 25.7, 24.2, 22.7. HRMS (ESI) for $C_{22}H_{24}N_3O_6S_2$ $[M - H]^-$ calcd 490.1112, found 490.1113.

https://doi.org/10.1021/jacsau.4c00868
JACS Au 2025, 5, 642−652

Synthesis of 2 (RSSS−ASA)

A double-neck round-bottom flask was charged with crude thiol **10** (290 mg, 1 mmol) and degassed THF (5 mL) and mixed using a stir bar. Activated thiol **6** (420 mg, 1.1 mmol) in degassed THF (5 mL) was added dropwise under an Ar atmosphere, resulting in a clear yellow solution. The reaction was stirred at room temperature overnight, with the reaction progress monitored by TLC. The solvent was removed under vacuum. The combined organic layers were washed with brine and dried over Na_2SO_4, filtered, and concentrated in a rotary evaporator. The crude product was purified by silica gel chromatography (DCM/MeOH = 100/1−10/1) to obtain **2** as a yellow solid (111 mg, 12% for two steps from 1.7 mmol of **9**). ^{1}H NMR (500 MHz, DMSO) δ 8.36−8.28 (m, 2H), 7.84 (dd, J = 8.7, 2.2 Hz, 1H), 7.79 (d, J = 8.1 Hz, 2H), 7.51 (d, J = 8.2 Hz, 2H), 6.82 (d, J = 8.8 Hz, 1H), 4.65 (d, J = 8.6 Hz, 1H), 4.24 (s, 2H), 3.65 (s, 3H), 1.90 (s, 3H), 1.38 (d, J = 13.5 Hz, 6H). ^{13}C NMR (126 MHz, DMSO) δ: 171.8, 170.7, 170.0, 164.5, 151.6, 144.8, 140.4, 131.0, 129.2, 126.2, 123.0, 118.8, 114.6, 58.4, 53.1, 52.3, 46.3, 42.1, 25.5, 24.3, 22.7. HRMS (ESI) for $C_{22}H_{24}N_3O_6S_3$ $[M - H]^-$ calcd 522.0833, found 522.0834.

Prodrug Release Assays

A 10 μL portion of each prodrug solution (1 mM) was transferred to a 5 mL polyethylene tube, followed by the addition of HPE-IAM solution (10 μL, 10 mM), colonic content suspension (980 μL), and dilution with PBS (1 mL). After vortexing for 30 s, the reaction was incubated at 37 °C. At a series of time points (0, 0.25, 0.5, 1, 2, 4, 6, 8, 12 h), 50 μL of the reaction solution was diluted with 150 μL of working solution containing internal standard compounds (IS). The solution was centrifuged twice at 18,000 rpm for 5 min at 4 °C to remove nonvisible impurities. 80 μL of the resulting supernatant was directly analyzed by LC-MS/MS, and the amount of compound was estimated from the standard curve. The above assays were repeated in triplicate and reported as the mean ± SD of three experiments. The LC-MS/MS analytical methods and the preparation of the colon content suspension are mentioned in the Supporting Information.

Cell Culture

Murine RAW264.7 macrophages were obtained from the Cell Bank of the Chinese Academy of Sciences (Shanghai, China). Cells were maintained in complete high-glucose Dulbecco's modified Eagle medium/nutrient mixture F-12 (DMEM/F-12; Gibco; Thermo Fisher Scientific Inc., Waltham, MA, USA) supplemented with 10% fetal bovine serum (FBS; Genetimes Technology Inc., Shanghai, China) and 1% penicillin−streptomycin (Gibco; Thermo Fisher Scientific Inc., Waltham, MA, USA) in an incubator containing 95% humidified air and 5% CO_2 at 37 °C. RAW 264.7 cells were incubated in 96-well plates (5×10^4 cells/well) at 37 °C for 24 h before the following assays.

A portion of cells was treated with LPS (1 μg/mL) and various concentrations of **RSS−ASA**, **RSSS−ASA**, or SASP (5, 25, and 125 μM) for 24 h at 37 °C. The supernatant medium was collected for the measurement of NO, IL-1β, IL-6, and MPO activities.

Measurements of NO, IL-1β, IL-6, and MPO Activities

For nitric oxide (NO) measurements, each reagent of the NO detection kit (Jiancheng Institute of Biotechnology, Nanjing, China) was added, and the OD value of each well was read at 540 nm.

The production of IL-1β or IL-6 in the supernatant was detected using the corresponding pro-inflammatory factor ELISA kits (Dakewe Biotech, China) in accordance with the manufacturer's guidelines. The results demonstrated that the prodrugs **RSS−ASA** and **RSSS−ASA** exhibited superior anti-inflammatory efficacy compared to the control drug SASP. This assay was conducted in triplicate, and the mean ± SD was recorded.

The activity of myeloperoxidase (MPO) was measured using commercial kits according to the manufacturer's instructions (Jiancheng Institute of Biotechnology, Nanjing, China). The absorbance was measured using a microplate reader (Synergy H1 Hybrid Multi-Mode Reader, BioTek Instruments Inc., Winooski, Vermont, USA).

Measurement of Intracellular Hypochlorite (ClO^-)

A portion of cells was treated with LPS (1 μg/mL) and **RSS−ASA**, **RSSS−ASA**, or SASP (125 μM) for 24 h at 37 °C. Then, cells were washed with PBS (200 μL × 3) to remove the culture medium. Subsequently, the cells were incubated with phorbol 12-myristate 13-acetate (PMA) (1 μg/mL, 200 μL) and **PZ−Py** (25 μM), a fluorescent probe, for 10 min. Afterward, the cells were washed with PBS (200 μL) twice to remove unloaded **PZ−Py**, and the intracellular endogenous hypochlorite level was measured according to the literature.[50]

Fluorescence imaging was performed with a Bioteck Lionheart X. Then, cells in 96-well plates were added to the cell lysis buffer (300 μL) to lyse the cells. The supernatant medium was collected for measuring the fluorometric intensity. The absorbance was measured at 550 nm using a microplate reader (Synergy H1 Hybrid Multi-Mode Reader, BioTek Instruments Inc., Winooski, Vermont, USA). The results are expressed as the mean ± SD (n = 6).

Measurement of Supersulfides

For the quantification of supersulfide levels by LC-MS/MS, HPE-IAM was chosen as the trapping agent (Scheme S6). The RAW 264.7 cell line was seeded in six-well cell culture plates (3.5×10^5 cells/well) and grown to confluence. Then DMSO, SASP, **RSS−ASA**, or **RSSS−ASA** (250 μM) was added to each well with serum-free MEM medium. After incubation at 37 °C for 2 h, the drug-containing medium was removed and cells were then washed with PBS three times and lysed in a cold 70% methanol solution of HPE-IAM (1 mM, 300 μL for each well). The mixture was vortexed for 5 min for more complete analyte abstract and protein precipitation and then centrifuged at 18,000 rpm for 5 min. An aliquot (100 μL) of the supernatant was transferred to a new tube, diluted with acetonitrile solution containing IS (100 μL, IS working solution), and recentrifuged at 18000 rpm before LC-MS/MS analysis. The protein content was measured using a BCA colorimetric protein kit. The LC-MS/MS analytical methods are described in the Supporting Information.

DSS-Induced Colitis in Mice

All animal protocols were approved by the Institutional Animal Care and Use Committee of China Pharmaceutical University (2024-07-058). Male C57BL/6 mice (8 weeks old) were purchased from Shanghai Super-B&K Laboratory Animal Co. (Shanghai, China). The mice were housed in pathogen-free conditions with controlled temperature (22−24 °C) and a 12 h/12 h light/dark cycle.

DSS was employed to induce colitis in mice. The mice were randomly assigned to one of four groups (n = 6 per group) as follows: a control group, a DSS-treated model group, an SASP group (0.2 mmol/kg), and a prodrug **RSSS−ASA** group (0.2 mmol/kg). The mice in the model group were administered a continuous 2.5% (w/v) DSS solution in drinking bottles for 8 consecutive days. Throughout the entirety of the adaptation and experimental phases, the mice in the control group were provided with drinking water. SASP and **RSSS−ASA** were suspended in 0.5% sodium carboxymethylcellulose (CMC-Na) and orally administered once a day for a period of 10 days.

Histopathological Analysis

The pathology of the colon tissue was observed using H&E staining. Fresh distal colon tissue was fixed in 4% paraformaldehyde for 48 h and subsequently embedded in paraffin. The H&E staining was performed on paraffin-embedded colon sections according to standard procedures. Histological images were captured with a light microscope (Olympus, Tokyo, Japan) for morphological analysis.

Enzyme-Linked Immunosorbent Assay (ELISA)

Mice plasma samples were incubated in a shaking table at 37 °C for 30 min. Following this, samples were centrifuged at 8000 rpm for 5 min to obtain the serum. The colon tissue samples were homogenized in normal saline and then centrifuged at 8000 rpm for 5 min to obtain the supernatants. The concentrations of IL-1β, IL-6, and TNF-α in the colonic supernatants and serum of mice were quantified using commercial kits (Elabscience, Wuhan, China) in accordance with the

https://doi.org/10.1021/jacsau.4c00868
JACS Au 2025, 5, 642−652

manufacturer's instructions. Additionally, the remaining colonic supernatant and serum samples were analyzed for the protein content, and the measured results were calibrated by the protein content, which was determined using a BCA Protein Assay Kit (Beyotime, China).

Tissue Distribution of Metabolites and Sulfane Sulfur

The mice were orally administered 0.1 mmol·kg^{-1} **RSSS−ASA**. Mice were anesthetized at 0.5, 2, 6, and 12 h after administration. Samples of the intestine, colon, and colon contents were harvested after perfusion with ice-cold saline and cut into pieces and snap-frozen. All sample preparations were preformed on ice. The samples (0.1 g) were homogenized with methanol (1 mL). The mixture was vortexed for 5 min for more complete analyte abstract and protein precipitation and then centrifuged at 18,000 rpm for 5 min. An aliquot (300 μL) of the supernatant was transferred to a new tube, diluted with methanol containing IS, and recentrifuged at 18,000 rpm for 5 min before LC-MS/MS analysis.

Blood samples were collected into tubes containing a sterile heparin sodium solution and immediately centrifuged at 8000 rpm for 5 min to obtain the plasma. The resulting plasma (50 μL) was transferred to a clean 1.5 mL polyethylene tube, and then 250 μL of ice-cold methanol containing IS was spiked into tubes for protein precipitation. All of the tubes were vortexed for 5 min and centrifuged at 18,000 rpm for 5 min. An aliquot (5 μL) of the supernatant was injected into the spectrophotometer for LC-MS/MS analysis.

For sulfane sulfur detection, the tissue samples (0.1 g) were homogenized with ice-cold PBS (1 mL, 50 mM, pH 7.4). The mixture was vortexed for 5 min and then centrifuged at 18,000 rpm for 5 min at 4 °C. An aliquot (300 μL) of the supernatant was transferred to a new tube and diluted with 190 μL of PBS. Then, 5 μL of cetyltrimethylammonium bromide solution (CTAB, 5 mM in ethanol) and 5 μL of SSP4 solution (1 mM in DMSO) were added. Samples were vortexed briefly and incubated in the dark at room temperature for 20 min before 200 μL was added to a black polystyrene 96-well plate. The fluorescence intensity was measured (Ex = 485 nm, Em = 525 nm) using a plate reader (BioTek SYNERGY H1 Multi-Mode Reader, Winooski, VT). To obtain the fluorescence intensity ratio, the fluorescence intensity measured in the colonic homogenate and colon content was, respectively, divided by the fluorescence intensity of the intestinal homogenate.

■ ASSOCIATED CONTENT

Supporting Information

The Supporting Information is available free of charge at https://pubs.acs.org/doi/10.1021/jacsau.4c00868.

Experimental procedures, supporting figures, analytical methods, cellular toxicity data, chemical synthesis and characterization data, and NMR and HRMS spectra (PDF)

■ AUTHOR INFORMATION

Corresponding Authors

Guangji Wang − *Key Laboratory of Drug Metabolism and Pharmacokinetics, China Pharmaceutical University, Nanjing, Jiangsu 210009, China*; Email: guangjiwang@hotmail.com

Le Zhen − *Key Laboratory of Drug Metabolism and Pharmacokinetics, China Pharmaceutical University, Nanjing, Jiangsu 210009, China*; orcid.org/0000-0002-1854-0764; Email: i_m_zhenle@163.com

Authors

Yu Zhang − *Key Laboratory of Drug Metabolism and Pharmacokinetics, China Pharmaceutical University, Nanjing, Jiangsu 210009, China*

Gao-Yao Cao − *Key Laboratory of Drug Metabolism and Pharmacokinetics, China Pharmaceutical University, Nanjing, Jiangsu 210009, China*

Zhihao Zhou − *Key Laboratory of Drug Metabolism and Pharmacokinetics, China Pharmaceutical University, Nanjing, Jiangsu 210009, China*

Tian-Yu Hu − *Key Laboratory of Drug Metabolism and Pharmacokinetics, China Pharmaceutical University, Nanjing, Jiangsu 210009, China*

Bi-Xin Xu − *Key Laboratory of Drug Metabolism and Pharmacokinetics, China Pharmaceutical University, Nanjing, Jiangsu 210009, China*

De-Ao Chen − *Key Laboratory of Drug Metabolism and Pharmacokinetics, China Pharmaceutical University, Nanjing, Jiangsu 210009, China*

Jin-Biao Du − *Key Laboratory of Drug Metabolism and Pharmacokinetics, China Pharmaceutical University, Nanjing, Jiangsu 210009, China*

Jiankun Wang − *Key Laboratory of Drug Metabolism and Pharmacokinetics, China Pharmaceutical University, Nanjing, Jiangsu 210009, China*

Complete contact information is available at: https://pubs.acs.org/10.1021/jacsau.4c00868

Author Contributions

▽Y.Z. and G.-Y.C. contributed equally. This manuscript was written through contributions of all authors. All authors have given approval to the final version of the manuscript. CRediT: **Yu Zhang** data curation, investigation, methodology, writing - original draft; **Gao-Yao Cao** data curation, investigation, methodology, validation, writing - original draft; **Zhihao Zhou** data curation, methodology; **Tian-Yu Hu** data curation, methodology; **Bi-Xin Xu** data curation, methodology; **De-Ao Chen** investigation; **Jin-Biao Du** data curation; **Jiankun Wang** funding acquisition, investigation, resources, writing - original draft; **Guangji Wang** funding acquisition, project administration, supervision; **Le Zhen** conceptualization, data curation, methodology, project administration, resources, supervision, validation, writing - review & editing.

Notes

The authors declare no competing financial interest.

■ ACKNOWLEDGMENTS

This work was supported by the National Natural Science Foundation of China (Grant Nos. 82173686, 81973186, and 81903707), the Outstanding Youth Foundation of Jiangsu Province (No. BK20200081), the Leading Technology Foundation Research Project of Jiangsu Province (No. BK20192005), and the Haihe Laboratory of Cell Ecosystem Innovation Fund (No. 22HHXBSS00005).

■ REFERENCES

(1) Barayeu, U.; Sawa, T.; Nishida, M.; Wei, F.-Y.; Motohashi, H.; Akaike, T. Supersulfide biology and translational medicine for disease control. *Br. J. Pharmacol.* **2023**, 1−16.

(2) Iciek, M.; Bilska-Wilkosz, A.; Gorny, M. Sulfane sulfur - new findings on an old topic. *Acta Biochim. Polym.* **2019**, *66*, 533−544.

(3) Pedre, B.; Barayeu, U.; Ezerina, D.; Dick, T. P. The mechanism of action of N-acetylcysteine (NAC): The emerging role of H_2S and sulfane sulfur species. *Pharmacol. Ther.* **2021**, *228*, No. 107916.

(4) Lau, N.; Pluth, M. D. Reactive sulfur species (RSS): persulfides, polysulfides, potential, and problems. *Curr. Opin. Chem. Biol.* **2019**, *49*, 1−8.
(5) Ono, K.; Akaike, T.; Sawa, T.; Kumagai, Y.; Wink, D. A.; Tantillo, D. J.; Hobbs, A. J.; Nagy, P.; Xian, M.; Lin, J.; Fukuto, J. M. Redox chemistry and chemical biology of H_2S, hydropersulfides, and derived species: Implications of their possible biological activity and utility. *Free Radical Biol. Med.* **2014**, *77*, 82−94.
(6) Filipovic, M. R.; Zivanovic, J.; Alvarez, B.; Banerjee, R. Chemical Biology of H_2S Signaling through Persulfidation. *Chem. Rev.* **2018**, *118*, 1253−1337.
(7) Cortese-Krott, M. M.; Koning, A.; Kuhnle, G. G. C.; Nagy, P.; Bianco, C. L.; Pasch, A.; Wink, D. A.; Fukuto, J. M.; Jackson, A. A.; van Goor, H.; Olson, K. R.; Feelisch, M. The Reactive Species Interactome: Evolutionary Emergence, Biological Significance, and Opportunities for Redox Metabolomics and Personalized Medicine. *Antioxid. Redox Signaling* **2017**, *27*, 684−712.
(8) Mishanina, A. V.; Libiad, M.; Banerjee, R. Biogenesis of reactive sulfur species for signaling by hydrogen sulfide oxidation pathways. *Nat. Chem. Biol.* **2015**, *11*, 457−464.
(9) Sekine, H.; Takeda, H.; Takeda, N.; Kishino, A.; Anzawa, H.; Isagawa, T.; Ohta, N.; Murakami, S.; Iwaki, H.; Kato, N.; Kimura, S.; Liu, Z.; Kato, K.; Katsuoka, F.; Yamamoto, M.; Miura, F.; Ito, T.; Takahashi, M.; Izumi, Y.; Fujita, H.; Yamagata, H.; Bamba, T.; Akaike, T.; Suzuki, N.; Kinoshita, K.; Motohashi, H. PNPO-PLP axis senses prolonged hypoxia in macrophages by regulating lysosomal activity. *Nat. Metab.* **2024**, *6*, 1108−1127.
(10) Ikeda-Imafuku, M.; Fukuta, T.; Chuang, V. T. G.; Sawa, T.; Maruyama, T.; Otagiri, M.; Ishida, T.; Ishima, Y. Acute Kidney Injury Caused by Rhabdomyolysis Is Ameliorated by Serum Albumin-Based Supersulfide Donors through Antioxidative Pathways. *Pharmaceuticals* **2024**, *17*, 128.
(11) Takeda, H.; Murakami, S.; Liu, Z.; Sawa, T.; Takahashi, M.; Izumi, Y.; Bamba, T.; Sato, H.; Akaike, T.; Sekine, H.; Motohashi, H. Sulfur metabolic response in macrophage limits excessive inflammatory response by creating a negative feedback loop. *Redox Biol.* **2023**, *65*, No. 102834.
(12) Kasamatsu, S.; Nishimura, A.; Alam, M. M.; Morita, M.; Shimoda, K.; Matsunaga, T.; Jung, M.; Ogata, S.; Barayeu, U.; Ida, T.; Nishida, M.; Nishimura, A.; Motohashi, H.; Akaike, T. Supersulfide catalysis for nitric oxide and aldehyde metabolism. *Sci. Adv.* **2023**, *9*, No. eadg8631.
(13) Iciek, M.; Bilska-Wilkosz, A.; Kozdrowicki, M.; Gorny, M. Reactive Sulfur Species in Human Diseases. *Antioxid. Redox Signaling* **2023**, *39*, 1000−1023.
(14) Fosnacht, K. G.; Cerda, M. M.; Mullen, E. J.; Pigg, H. C.; Pluth, M. D. Esterase-Activated Perthiocarbonate Persulfide Donors Provide Insights into Persulfide Persistence and Stability. *ACS Chem. Biol.* **2022**, *17*, 331.
(15) Aggarwal, S. C.; Khodade, V. S.; Porche, S.; Pharoah, B. M.; Toscano, J. P. Photochemical Release of Hydropersulfides. *J. Org. Chem.* **2022**, *87*, 12644.
(16) Khodade, V. S.; Aggarwal, S. C.; Pharoah, B. M.; Paolocci, N.; Toscano, J. P. Alkylsulfenyl thiocarbonates: precursors to hydropersulfides potently attenuate oxidative stress. *Chem. Sci.* **2021**, *12*, 8252.
(17) Khodade, V. S.; Pharoah, B. M.; Paolocci, N.; Toscano, J. P. Alkylamine-Substituted Perthiocarbamates: Dual Precursors to Hydropersulfide and Carbonyl Sulfide with Cardioprotective Actions. *J. Am. Chem. Soc.* **2020**, *142*, 4309.
(18) Dillon, K. M.; Carrazzone, R. J.; Wang, Y.; Powell, C. R.; Matson, J. B. Polymeric Persulfide Prodrugs: Mitigating Oxidative Stress through Controlled Delivery of Reactive Sulfur Species. *ACS Macro. Lett.* **2020**, *9*, 606.
(19) Chaudhuri, A.; Venkatesh, Y.; Das, J.; Gangopadhyay, M.; Maiti, T. K.; Singh, N. D. P. One- and Two-Photon-Activated Cysteine Persulfide Donors for Biological Targeting. *J. Org. Chem.* **2019**, *84*, 11441.
(20) Khodade, V. S.; Toscano, J. P. Development of S-Substituted Thioisothioureas as Efficient Hydropersulfide Precursors. *J. Am. Chem. Soc.* **2018**, *140*, 17333.
(21) Kang, J.; Xu, S.; Radford, M. N.; Zhang, W.; Kelly, S. S.; Day, J. J.; Xian, M. O-S Relay Deprotection: A General Approach to Controllable Donors of Reactive Sulfur Species. *Angew. Chem., Int. Ed.* **2018**, *57*, 5893.
(22) Yuan, Z.; Zheng, Y.; Yu, B.; Wang, S.; Yang, X.; Wang, B. Esterase-Sensitive Glutathione Persulfide Donor. *Org. Lett.* **2018**, *20*, 6364.
(23) Zheng, Y.; Yu, B.; Li, Z.; Yuan, Z.; Organ, C. L.; Trivedi, R. K.; Wang, S.; Lefer, D. J.; Wang, B. An Esterase-Sensitive Prodrug Approach for Controllable Delivery of Persulfide Species. *Angew. Chem., Int. Ed.* **2017**, *56*, 11749.
(24) Artaud, I.; Galardon, E. A Persulfide Analogue of the Nitrosothiol SNAP: Formation, Characterization and Reactivity. *ChemBioChem.* **2014**, *15*, 2361.
(25) Xu, B.-X.; Hu, T.-Y.; Du, J.-B.; Xie, T.; Xu, Y.-W.; Jin, X.; Xu, S.-T.; Jin, H.-W.; Wang, G.; Wang, J.; Zhen, L. In pursuit of feedback activation: New insights into redox-responsive hydropersulfide prodrug combating oxidative stress. *Redox Biol.* **2024**, *72*, No. 103130.
(26) Choudhary, B. S.; Kumar, T. A.; Vashishtha, A.; Tejasri, S.; Kumar, A. S.; Agarwal, R.; Chakrapani, H. An esterase-cleavable persulfide donor with no electrophilic byproducts and a fluorescence reporter. *Chem. Commun.* **2024**, *60*, 1727−1730.
(27) Bora, P.; Sathian, M. B.; Chakrapani, H. Enhancing cellular sulfane sulfur through β-glycosidase-activated persulfide donors: mechanistic insights and oxidative stress mitigation. *Chem. Commun.* **2022**, *58*, 2987−2990.
(28) Xu, Y.-W.; Xu, B.-X.; Wang, J.; Jin, H.-W.; Xu, S.-T.; Wang, G.; Zhen, L. Peroxynitrite-Promoted Persulfide Prodrugs with Protective Potential against Paracetamol Poisoning. *Chem. − Eur. J.* **2022**, *28*, No. e202200540.
(29) Dillon, K. M.; Morrison, H. A.; Powell, C. R.; Carrazzone, R. J.; Ringel-Scaia, V. M.; Winckler, E. W.; Council-Troche, R. M.; Allen, I. C.; Matson, J. B. Targeted Delivery of Persulfides to the Gut: Effects on the Microbiome. *Angew. Chem., Int. Ed.* **2021**, *60*, 6061.
(30) Hankins, R. A.; Suarez, S. I.; Kalk, M. A.; Green, N. M.; Harty, M. N.; Lukesh, J. C., 3rd An Innovative Hydrogen Peroxide-Sensing Scaffold and Insight Towards its Potential as an ROS-Activated Persulfide Donor. *Angew. Chem., Int. Ed.* **2020**, *59*, 22238.
(31) Wang, Y.; Dillon, K. M.; Li, Z.; Winckler, E. W.; Matson, J. B. Alleviating Cellular Oxidative Stress through Treatment with Superoxide-Triggered Persulfide Prodrugs. *Angew. Chem., Int. Ed.* **2020**, *59*, 16698.
(32) Bora, P.; Chauhan, P.; Manna, S.; Chakrapani, H. A Vinyl-Boronate Ester-Based Persulfide Donor Controllable by Hydrogen Peroxide, a Reactive Oxygen Species (ROS). *Org. Lett.* **2018**, *20*, 7916.
(33) Powell, C. R.; Dillon, K. M.; Wang, Y.; Carrazzone, R. J.; Matson, J. B. A Persulfide Donor Responsive to Reactive Oxygen Species: Insights into Reactivity and Therapeutic Potential. *Angew. Chem., Int. Ed.* **2018**, *57*, 6324.
(34) Yu, B.; Kang, T.; Xu, Y.; Liu, Y.; Ma, Y.; Ke, B. Prodrugs of Persulfide and Sulfide: Is There a Pharmacological Difference between the Two in the Context of Rapid Exchanges among Various Sulfur Species In Vivo? *Angew. Chem., Int. Ed.* **2022**, *61*, No. e202201668.
(35) Wu, Z.; Khodade, V. S.; Chauvin, J.-P. R.; Rodriguez, D.; Toscano, J. P.; Pratt, D. A. Hydropersulfides Inhibit Lipid Peroxidation and Protect Cells from Ferroptosis. *J. Am. Chem. Soc.* **2022**, *144*, 15825−15837.
(36) Akaike, T.; Ida, T.; Wei, F.-Y.; Nishida, M.; Kumagai, Y.; Alam, M. M.; Ihara, H.; Sawa, T.; Matsunaga, T.; Kasamatsu, S.; Nishimura, A.; Morita, M.; Tomizawa, K.; Nishimura, A.; Watanabe, S.; Inaba, K.; Shima, H.; Tanuma, N.; Jung, M.; Fujii, S.; Watanabe, Y.; Ohmuraya, M.; Nagy, P.; Feelisch, M.; Fukuto, J. M.; Motohashi, H. Cysteinyl-tRNA synthetase governs cysteine polysulfidation and mitochondrial bioenergetics. *Nat. Commun.* **2017**, *8*, 1177.

https://doi.org/10.1021/jacsau.4c00868
JACS Au 2025, 5, 642−652

(37) Ida, T.; Sawa, T.; Ihara, H.; Tsuchiya, Y.; Watanabe, Y.; Kumagai, Y.; Suematsu, M.; Motohashi, H.; Fujii, S.; Matsunaga, T.; Yamamoto, M.; Ono, K.; Devarie-Baez, N. O.; Xian, M.; Fukuto, J. M.; Akaike, T. Reactive cysteine persulfides and S-polythiolation regulate oxidative stress and redox signaling. *Proc. Natl. Acad. Sci. U. S. A.* **2014**, *111*, 7606−7611.
(38) Weinreb, R. N.; Sforzolini, B. S.; Vittitow, J.; Liebmann, J. Latanoprostene bunod 0.024% versus timolol maleate 0.5% in subjects with open-angle glaucoma or ocular hypertension: the APOLLO study. *Ophthalmology* **2016**, *123*, 965−973.
(39) Fiorucci, S.; Orlandi, S.; Mencarelli, A.; Caliendo, G.; Santagada, V.; Distrutti, E.; Santucci, L.; Cirino, G.; Wallace, J. L. Enhanced activity of a hydrogen sulphide-releasing derivative of mesalamine (ATB-429) in a mouse model of colitis. *Br. J. Pharmacol.* **2007**, *150*, 996−1002.
(40) Ryan, A. Azoreductases in drug metabolism. *Br. J. Pharmacol.* **2017**, *174*, 2161−2173.
(41) Chourasia, M. K.; Jain, S. K. Pharmaceutical approaches to colon targeted drug delivery systems. *J. Pharm. Pharm. Sci.* **2003**, *6*, 33−66.
(42) Ragunath, K.; Williams, J. G. Review article: balsalazide therapy in ulcerative colitis. *Aliment. Pharmacol. Ther.* **2001**, *15*, 1549−1554.
(43) Klotz, U.; Maier, K.; Fischer, C.; Heinkel, K. Therapeutic efficacy of sulfasalazine and its metabolites in patients with ulcerative colitis and Crohn's disease. *N. Engl. J. Med.* **1980**, *303*, 1499−1502.
(44) Mehta, R. S.; Mayers, J. R.; Zhang, Y.; Bhosle, A.; Glasser, N. R.; Nguyen, L. H.; Ma, W.; Bae, S.; Branck, T.; Song, K.; Sebastian, L.; Pacheco, J. A.; Seo, H.-S.; Clish, C.; Dhe-Paganon, S.; Ananthakrishnan, A. N.; Franzosa, E. A.; Balskus, E. P.; Chan, A. T.; Huttenhower, C. Gut microbial metabolism of 5-ASA diminishes its clinical efficacy in inflammatory bowel disease. *Nat. Med.* **2023**, *29*, 700−709.
(45) Hickman, D.; Pope, J.; Patil, S. D.; Fakis, G.; Smelt, V.; Stanley, L. A.; Payton, M.; Unadkat, J. D.; Sim, E. Expression of arylamine N-acetyltransferase in human intestine. *Gut* **1998**, *42*, 402−409.
(46) Sim, E.; Walters, K.; Boukouvala, S. Arylamine N-acetyltransferases: From structure to function. *Drug Metab. Rev.* **2008**, *40*, 479−510.
(47) Iciek, M.; Wlodek, L. Biosynthesis and biological properties of compounds containing highly reactive, reduced sulfane sulfur. *Polym. J. Pharmacol.* **2001**, *53*, 215−225.
(48) Lin, W.; Chen, H.; Chen, X.; Guo, C.; Manea, A.; Manda, G. The Roles of Neutrophil-Derived Myeloperoxidase (MPO) in Diseases: The New Progress. *Antioxidants* **2024**, *13*, 132.
(49) Aratani, Y. Myeloperoxidase: Its role for host defense, inflammation, and neutrophil function. *Arch. Biochem. Biophys.* **2018**, *640*, 47−52.
(50) Xiao, H.; Xin, K.; Dou, H.; Yin, G.; Quan, Y.; Wang, R. A fast-responsive mitochondria-targeted fluorescent probe detecting endogenous hypochlorite in living RAW 264.7 cells and nude mouse. *Chem. Commun.* **2015**, *51*, 1442−1445.
(51) Shieh, M.; Ni, X.; Xu, S.; Lindahl, S. P.; Yang, M.; Matsunaga, T.; Flaumenhaft, R.; Akaike, T.; Xian, M. Shining a light on SSP4: A comprehensive analysis and biological applications for the detection of sulfane sulfurs. *Redox Biol.* **2022**, *56*, No. 102433.
(52) Shieh, M.; Xu, S.; Lederberg, O. L.; Xian, M. Detection of sulfane sulfur species in biological systems. *Redox Biol.* **2022**, *57*, No. 102502.

https://doi.org/10.1021/jacsau.4c00868
JACS Au 2025, 5, 642−652